Contribution from the Department of Chemistry and Biochemistry,
University of Windsor, Windsor, Ontario N9B 3P4, Canada

EPR and NMR Study of the Spin-Crossover Transition in Fe(4,4'-bi-1,2,4-triazole)$_2$(SCN)$_2$·H$_2$O and Fe(4,4'-bi-1,2,4-triazole)$_2$(SeCN)$_2$·H$_2$O. X-ray Structure Determination of Fe(4,4'-bi-1,2,4-triazole)$_2$(SeCN)$_2$·H$_2$O

Andrzej Ozarowski, Yu Shunzhong,[†] Bruce R. McGarvey,* Anil Mislankar, and John E. Drake

EPR and proton NMR studies have been done on the spin-crossover transition in Fe(4,4'-bi-1,2,4-triazole)$_2$(SCN)$_2$·H$_2$O and the related selenocyanate compound. The new selenocyanate compound was found to have the transition temperatures of T(up) = 217 K and T(down) = 211 K, and the room-temperature X-ray structure was obtained. The compound, which crystallizes as monoclinic in the space group $C2/c$ (No. 15), has the cell parameters a = 11.342 (2) Å, b = 13.169 (3) Å, c = 13.118 (4) Å, β 91.79 (2)°, v = 1959 (1) Å^3, Z = 4, R = 0.0467, and R_w = 0.0477. EPR spectra of Cu^{2+} and Mn^{2+} doped into single crystals of Fe(4,4'-bi-1,2,4-triazole)$_2$(SCN)$_2$·H$_2$O show only one magnetic site in the diamagnetic phase, indicating a change in structure from the paramagnetic phase. All single crystals pulverized spontaneously when warmed from the diamagnetic to the paramagnetic region of temperature. In the diamagnetic phase of Fe(4,4'-bi-1,2,4-triazole)$_2$(SCN)$_2$·H$_2$O, the spin Hamiltonian parameters for Cu^{2+} were found to be $g_\parallel$ = 2.280, $g_\perp$ = 2.057, $A_\parallel$ = 177 × 10^{-4} cm^{-1}, and $A_\perp \approx 0$ and for Mn^{2+} were g = 2.0, D 0.12 cm^{-1}, and a = –0.0018 cm^{-1}. Similar parameters were obtained from powder spectra for the same ions doped into Fe(4,4'-bi-1,2,4-triazole)$_2$(SeCN)$_2$·H$_2$O. Proton NMR spectra of Fe(4,4'-bi-1,2,4-triazole)$_2$(SCN)$_2$·H$_2$O, Fe(4,4'-bi-1,2,4-triazole)$_2$(SeCN)$_2$·H$_2$O, and Fe(4,4'-bi-1,2,4-triazole)$_2$(SCN)$_2$ (dehydrated) were obtained over a large range of temperatures, and the room-temperature spectrum of the related compound Co(4,4'-bi-1,2,4-triazole)$_2$(SCN)$_2$·H$_2$O was also obtained. In the paramagnetic samples, the simulations of the NMR powder spectra yielded iron–proton distances for the hydrogen atom closest to the iron atom and the water hydrogen. Simulations for the diamagnetic samples showed the water molecule to exhibit a Pake doublet from which the H–H distance was deduced. The existence of this Pake doublet in the diamagnetic phase indicated lack of mobility for the water protons, which was contrary to what was found from the simulations in the paramagnetic phase. Simulations of the experimental NMR spectra in the spin-crossover region demonstrated unequivocally that the transition must occur in domains rather than in a statistically random fashion.

Introduction

The temperature-dependent spin-crossover transition $^5T \leftrightarrow {}^1A$ in Fe(btr)$_2$(SCN)$_2$·H$_2$O (btr = 4,4'-bi-1,2,4-triazole) was first reported by Vreugdenhil et al.,[1] in which the transition was detected by magnetic susceptibility measurements. It has since been studied by using Mössbauer and Cu^{2+} EPR[2] spectroscopy. The transition is abrupt, with a hysteresis occurring at 123.5 K on cooling and at 144.5 K on warming. Under vacuum, the sample was found to lose the water of hydration very easily during the transition. The dehydrated compound was found to be paramagnetic at all temperatures studied (85–295 K). Figg and Herber[3] have also measured the transition with magnetic susceptibility and FTIR and report the transition temperatures to be 123 and 140 K.

Many iron(II) compounds exhibit the spin-crossover phenomena in the solid state and have been the subject of many studies.[4,5] EPR studies of the transition have been done by doping the compound with small percentages of Mn^{+2} and sometimes Cu^{+2} and detecting the EPR spectrum of the dopant.[6–10] Although EPR studies of powders[6,8] have yielded some information and can be used to detect the transition, the EPR studies of single crystals[7,9,10] have yielded the most information about the nature of the transition.

Due to the short lifetime of the spin state in the paramagnetic ^5T state of Fe^{2+}, it is possible to detect the proton NMR in the paramagnetic phase as well as the diamagnetic phase of the spin-crossover compounds. Previous NMR studies[6,11,12] have shown that the powder NMR spectrum in the paramagnetic phase is distinctly anisotropic in shape due to the magnetic dipolar interaction between the nucleus and the paramagnetic iron ions. The width of the paramagnetic spectrum increases with decreasing temperature following the Curie law, making it easy to determine the spin-crossover transition by the decrease in line width when the conversion to the diamagnetic phase occurs. In addition to line shapes, NMR studies of the proton T_1 as a function of temperature have been done.[11,12] The systems for which T_1 has been measured have all had a temperature-independent T_1 of approximately 3 ms in the paramagnetic phase and a much longer but highly temperature dependent T_1 in the diamagnetic phase.

The NMR spectrum of spin-crossover compounds has been of little value in determining much about the transition, except to detect the transition itself from the line width change. Little information has been extracted from the anisotropic shape of the paramagnetic resonance due to the large number of different protons in the ligands studied. Single-crystal studies would be useful, but the size of crystal needed for NMR is not easy to achieve for the systems studied, heretofore. This work was undertaken because the Fe(btr)$_2$(SCN)$_2$·H$_2$O system appeared to be an ideal system for an NMR study due to the small number of distinct types of protons in the ligand. The free btr ligand has only one type of proton in solution NMR spectra but these become two distinct types when complexed to the iron ion due to the different distances from the iron atom. In the solid there will be a third type of proton in the water molecule. In the paramagnetic phase, the iron–proton distances are significantly different for these three protons and this will give rise to three anisotropic powder spectra that do not completely overlap each other, making it possible by simulation studies to extract separate shift parameters

---

*To whom all correspondence should be addressed.
†Present address: Department of Chemistry, Xinjiang University, Wulumuqi, People's Republic of China.

(1) Vreugdenhil, W.; Gorter, S.; Haasnoot, J. G.; Reedijk, J. *Polyhedron* **1985**, *4*, 1769.
(2) Vreugdenhil, W.; van Diemen, J. H.; de Graaf, A. G.; Haasnoot, J. G.; Reedijk, J.; van der Kraan, A. M.; Kahn, O.; Zarembowitch, J. *Polyhedron* **1990**, *9*, 2971.
(3) Figg, D. C.; Herber, R. H. Chemistry Department, Rutgers University. Private communication.
(4) Gütlich, P. *Struct. Bonding (Berlin)* **1981**, *44*, 83.
(5) (a) König, E.; Ritter, G.; Kulshreshtha, S. K. *Chem. Rev.* **1985**, *85*, 219. (b) König, E. *Prog. Inorg. Chem.* **1987**, *35*, 527.
(6) Rao, P. S.; Reuveni, A.; McGarvey, B. R.; Ganguli, P.; Gütlich, P. *Inorg. Chem.* **1981**, *20*, 204.
(7) Ozarowski, A.; McGarvey, B. R.; Sarkar, A. B.; Drake, J. E. *Inorg. Chem.* **1988**, *27*, 628.
(8) Vreugdenhil, W.; Haasnoot, J. G.; Kahn, O.; Theury, P.; Reedijk, J. *J. Am. Chem. Soc.* **1987**, *109*, 5272.
(9) Ozarowski, A.; McGarvey, B. R. *Inorg. Chem.* **1989**, *28*, 2262.
(10) Doan, P. E.; McGarvey, B. R. *Inorg. Chem.* **1990**, *29*, 874.
(11) Rao, P. S.; Ganguli, P.; McGarvey, B. R. *Inorg. Chem.* **1981**, *20*, 3682.
(12) Maiti, B.; McGarvey, B. R.; Rao, P. S.; Stubbs, L. S. *J. Magn. Reson.* **1983**, *54*, 99.

Table I. Crystallographic Data for $Fe(btr)_2(SeCN)_2 \cdot H_2O$

chem formula: $C_{10}H_{10}N_{14}OSe_2Fe$	fw = 556.06
$a = 11.342 (2)$ Å	space group: $C2/c$ (No. 15)
$b = 13.169 (3)$ Å	$T = 24$ °C
$c = 13.118 (4)$ Å	$\lambda = 0.71069$ Å
$\beta = 91.79 (2)°$	$\rho_{obsd} = 1.87$ g cm^{-3}
$V = 1959 (1)$ Å^3	$\rho_{calcd} = 1.88$ g cm^{-3}
$Z = 4$	$\mu = 43.79$ cm^{-1}
$R = 0.0467$	transm coeff = 0.60–0.71
$R_w = 0.0477$	

for individual types of protons in the sample. In addition, there was the possibility of determing T_1 (from a powder sample) for a single proton at specific orientations in the magnetic field for the paramagnetic phase, which has not been done before to our knowledge. In fact, there appears to be virtually no studies of T_1 in purely paramagnetic solids.

In this paper, we report on a combined EPR and NMR study of $Fe(btr)_2(SCN)_2 \cdot H_2O$ over a range of temperatures that span the spin-crossover transition. In addition, we studied the dehydrated $Fe(btr)_2(SCN)_2$, which is paramagnetic at all temperatures but has only two distinct protons in the solid state. Also, we have synthesized the $Fe(btr)_2(SeCN)_2 \cdot H_2O$ compound and report here on its spin-crossover characteristics as determined from EPR and NMR studies. Significant differences between the selenocyanato and thiocyanato versions of the compound suggested to us that it would be also useful to have the crystal structure of $Fe(btr)_2(SeCN)_2 \cdot H_2O$ to compare with those of $Fe(btr)_2(SCN)_2 \cdot H_2O$ and $Co(btr)_2(SCN)_2 \cdot H_2O$. We have, therefore, done an X-ray crystal structure of $Fe(btr)_2(SeCN)_2 \cdot H_2O$.

Experimental Section

Structure Determination and Refinement. Suitable crystals of $Fe(btr)_2(SeCN)_2 \cdot H_2O$ were sealed in a capillary tube and mounted on a Syntex P2$_1$ four-circle diffractometer equipped with a scintillation counter and graphite monochromator. The unit cell dimensions, listed in Table I, were obtained from a least-squares refinement of the setting angles of 15 reflections in the $15 < 2\theta < 35°$ range. The space group $C2/c$ was used and later assumed correct because of the successful refinement of the structure. The data were collected by using the θ-2θ scan technique in a manner described in detail elsewhere;[13] the details of other pertinent X-ray data are given in Table I. The stability of the crystals in the X-ray beam was monitored by 3 reflections measured after every 100 reflections and no significant change in the intensities were noted. The data were corrected for Lorentz and polarization effects, and an empirical absorption correction was applied. The Fe atom was located by assuming the compound was isomorphous with $Co(btr)_2(SCN)_2 \cdot H_2O^1$ and then a series of subsequent difference Fourier maps revealed the positions of all the remaining non-hydrogen atoms. The structure was refined by using a full-matrix least-squares refinement procedure, with anisotropic structure factors assigned to all non-hydrogen atoms. The occupancy numbers of the two positions of Se and Se* were adjusted so that the values of U_{eq} were identical for the Se atoms in the two positions. This resulted in occupancies of 0.78 and 0.22, respectively, for Se and Se*. The hydrogen atoms were included in the positions indicated by the least-squares refinement, with isotropic U's set at 0.1 Å^2 greater than that of the corresponding carbon atom. For the hydrogen atoms attached to oxygen, U was set at 0.90 Å^2, which was slightly higher than the minimum value required to allow convergence. Least-squares refinement minimizing the function $\sum w(|F_o| - |F_c|)^2$ converged at $R = \sum (||F_o| - |F_c||)^2 / \sum |F_o| = 0.0467$ and $R_w = [\sum w(||F_o| - |F_c||)^2/|F_o|^2]^{1/2} = 0.0477$. A final ρ value of 0.001 717 was employed for the weighting scheme $w = 1/\sum[\sigma^2(F) + \rho F^2]$. In the last cycle, no parameters changed by more than 0.002σ. The largest residual peaks were of no chemical significance, being 1.05, 0.97, and 0.92 Å respectively from Fe, Se, and Se*. No evidence of secondary extinction was found. Sources of computer programs and scattering factors have been previously described.[13]

Preparation of $Fe(btr)_2(SCN)_2 \cdot H_2O$ and $Fe(btr)_2(SeCN)_2 \cdot H_2O$. The ligand bitriazole was prepared from formic acid and hydrazine as described by Haasnoot and Groeneveld.[14] A hot solution containing $FeCl_2 \cdot 4H_2O$ (5 mmol) and NH_4SCN or $KSeCN$ (10 mmol) in 20 mL of H_2O was mixed with a solution of 10 mmol of bitriazole in 20 mL of H_2O. The hot mixture was filtered and put into a refrigerator. After the mixture was cooled, the white crystalline precipitate was filtered off

Table II. Final Fractional Coordinates and Isotropic Thermal Parameters for Non-Hydrogen Atoms of $Fe(btr)_2(SeCN)_2 \cdot H_2O$ with Standard Deviations in Parentheses

atom	x	y	z	U_{eq},^{a} Å$^2 \times 10^3$
Fe	0.2500	0.2500	0.0000	25.3 (6)
Se	0.6476 (3)	0.3687 (2)	0.1111 (3)	62 (2)
Se*	0.628 (1)	0.4063 (6)	0.1031 (9)	62 (6)
N	0.4316 (4)	0.2711 (4)	0.0355 (4)	41 (3)
C	0.5136 (5)	0.3122 (4)	0.0658 (4)	37 (3)
N11	0.2786 (4)	−0.0958 (3)	0.4517 (3)	31 (2)
N12	0.3683 (4)	−0.0331 (3)	0.4904 (3)	37 (3)
C13	0.3611 (5)	0.0511 (4)	0.4382 (4)	35 (3)
N14	0.2726 (4)	0.0449 (3)	0.3687 (3)	33 (3)
C15	0.2228 (5)	−0.0473 (4)	0.3786 (4)	37 (4)
N21	0.2259 (4)	0.1988 (3)	0.1561 (3)	32 (3)
N22	0.1380 (4)	0.2344 (4)	0.2178 (3)	45 (3)
C23	0.1489 (6)	0.1837 (5)	0.3028 (4)	46 (4)
N24	0.2378 (4)	0.1171 (3)	0.2968 (3)	32 (3)
C25	0.2835 (5)	0.1285 (4)	0.2038 (4)	35 (3)
O	0.0000	0.4404 (7)	0.2500	123 (10)

^{a} U_{eq} is defined as one-third of the trace of the orthogonal U_{ij} tensor.

and recrystallized from hot water. A small amount of $CuCl_2 \cdot 4H_2O$ (Cu/Fe = 0.01) was added to the reaction mixture to obtain copper doped samples. $Co(btr)_2(SCN)_2 \cdot H_2O$, $Mn(btr)_2(SCN)_2 \cdot H_2O$, and $Mn(btr)_2(SeCN)_2 \cdot H_2O$ were prepared in the same way.

Preparation of Crystals. Large crystals of $Fe(btr)_2(SCN)_2 \cdot H_2O$ doped with Mn(II) suitable for EPR were obtained by dissolving 0.2 g of the iron complex and 0.01 g of the Mn complex in 40 mL of water at room temperature and allowing the solution to evaporate over a period of several weeks. All attempts to prepare large crystals of the selenocyanate complex have failed because of the instability of its solutions over a long period of time. Small X-ray quality single-crystals of $Fe(btr)_2(SeCN)_2 \cdot H_2O$ were obtained by blowing a very slow stream of nitrogen for 1 week over a saturated aqueous solution of the compound placed into a dark flask.

EPR and NMR Spectroscopy. EPR spectra were taken with a Varian E12 spectrometer equipped with a cylindrical cavity and rotating magnet. The magnetic field sweeps were calibrated by proton NMR spectroscopy. Variable-temperature spectra were obtained by using the Varian variable-temperature accessory using cooled N_2 gas.

NMR spectra were taken by a Bruker CXP90 FT spectrometer. Powder samples were placed in spherical sealed glass containers to minimize internal magnetic susceptibility shifts in the paramagnetic samples. The NMR spectra were obtained by using a solid-state echo pulse sequence to avoid dead time problems. The 90° pulse time for protons was 2.5 μs. T_1 measurements were obtained by using the modified inversion–recovery method suggested by Frye,[15] which gives a decay to zero and requires only a two-parameter fit for exponential decays. This inversion–recovery pulse scheme was combined with the solid-state echo sequence to give resonance signals of undistorted shape. Variable-temperature spectra were acquired by using the Bruker cooled N_2 gas system, which was modified to allow temperatures as low as 100 K. The temperature was calibrated by using a copper–constatan thermocouple. The temperatures reported should be correct to ±2 K.

Results

The X-ray structure determination of the isomorphous compound $Co(btr)_2(SCN)_2 \cdot H_2O$ has been reported earlier[1] and that of $Fe(btr)_2(SCN)_2 \cdot H_2O$ very recently.[2] We were able to grow suitable crystals of $Fe(btr)_2(SeCN)_2 \cdot H_2O$ and perform an X-ray structure determination to compare with the other systems. The single crystals of $Fe(btr)_2(SeCN)_2 \cdot H_2O$ maintained their integrity when cooled down through the spin-crossover transition but instantly pulverized every time the crystal was warmed back up through the transition.

Both $Fe(btr)_2(SCN)_2 \cdot H_2O$ and $Fe(btr)_2(SeCN)_2 \cdot H_2O$ were prepared with $\approx$1% Mn^{+2} and Cu^{+2} dopings and their powder EPR spectra taken. EPR spectra of doped single crystals of $Fe(btr)_2(SCN)_2 \cdot H_2O$ were obtained both above and below the spin-crossover transition temperatures. It was also possible to acquire proton NMR spectra of both $Fe(btr)_2(SCN)_2 \cdot H_2O$ and $Fe(btr)_2(SeCN)_2 \cdot H_2O$ in powder form at all temperatures.

(13) Chadha, R. K.; Drake, J. E.; Sarkar, A. B. *Inorg. Chem.* **1986**, *25*, 2201.
(14) Haasnoot, J. G.; Groeneveld, W. L. *Z. Naturforsch.* **1979**, *34B*, 1500.

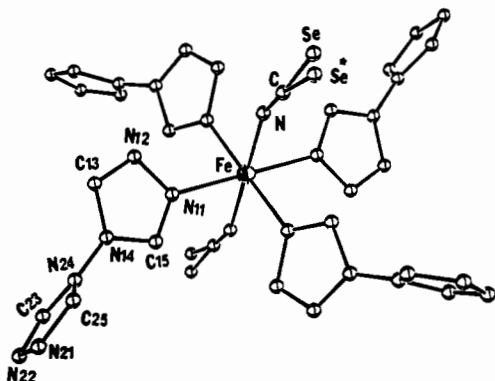(15) Frye, J. S. *Concepts Magn. Reson.* **1989**, *1*, 27.

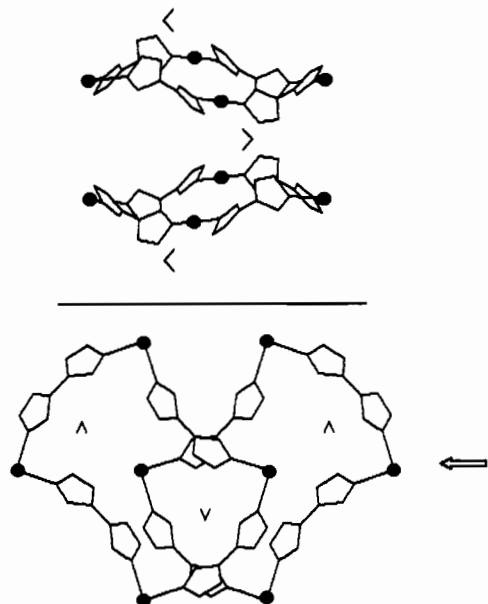**Figure 1.** ORTEP diagram for $Fe(btr)_2(SeCN)_2 \cdot H_2O$ showing the immediate environment about Fe.

Figure 2. Stick diagram showing layer structure of $Fe(btr)_2(SeCN)_2 \cdot H_2O$. The diagram shows two $Fe_4(btr)_4$ units in two planes with the solid circles being Fe atoms. The bottom diagram is a view looking directly down on the layers. The top is a perspective slightly off from that of the arrow in the lower diagram. The water molecules between the layers are also shown. The $SeCN^-$ ions have been omitted for clarity.

A. Description of the Structure of $Fe(btr)_2(SeCN)_2 \cdot H_2O$. Final atomic coordinates for non-hydrogen atoms are given in Table II, important distances and bond angles are given in Table III, and an ORTEP diagram is given in Figure 1, illustrating the immediate environment about Fe. Figure 2 shows part of the two-dimensional layer structure using a stick diagram. The coordination polyhedron around iron is a distorted octahedron with the two selenocyanate groups trans to each other. The Fe–NCSe distance of 2.116 (5) Å is slightly longer than that found to be typical for Fe–NCS systems and the 2.098 (2) Å in $Co(btr)_2$-$(SCN)_2 \cdot H_2O$[1] but shorter than the Fe–NCS distance of 2.125 Å in $Fe(btr)_2(SCN)_2 \cdot H_2O$.[2] As was found for $Co(btr)_2(SCN)_2 \cdot H_2O$,[1] the Fe–N–C angle, 156.8 (4)°, differs significantly from 180°. The remaining four positions of the coordination polyhedron are occupied by the N atoms of the ligands at angles ranging from 88.0 (2) to 91.9 (2)° and Fe–N distances ranging from 2.156 (4) to 2.181 (4) Å. The ranges are slightly larger than those reported for the related cobalt complex.[1] The similarity between these two compounds extends to the location of the water molecule and the differences in the position of the chalcogenide atoms in the disorder for that atom. As with the cobalt compound, one N–C–chalcogen bond is close to linear and the other more obviously bent so that N–C–Se is 176.0 (5)° and N–C–Se* is 166.2°. However in $Fe(btr)_2(SeCN)_2 \cdot H_2O$, the higher occupancy site has a nearly linear relationship in contrast to that noted for the cobalt compound, although the relative occupancies are both close to 80/20.

Interatomic Distances			
Fe–N	2.116 (5)	N–C	1.138 (7)
Fe–N11	2.156 (4)	C–Se	1.778 (7)
Fe–N21	2.181 (4)	C–Se*	1.85 (1)
N11–N12	1.394 (6)	N21–N22	1.385 (6)
N12–C13	1.305 (7)	N22–C23	1.302 (7)
C13–N14	1.336 (7)	C23–N24	1.340 (8)
N14–C15	1.346 (7)	N24–C25	1.350 (7)
C15–N11	1.300 (7)	C25–N21	1.284 (7)
C13–H13	0.85 (6)	C23–H23	0.99 (7)
C15–H15	0.99 (6)	C25–H25	0.89 (6)
N14–N24	1.389 (6)		

Interatomic Angles			
N–Fe–N'11	88.0 (2)	Fe–N–C	156.8 (4)
N–Fe–N21	89.1 (2)	N–C–Se	176.0 (5)
N'11–Fe–N21	89.5 (2)	N–C–Se*	166.2 (5)
N'11–Fe–N	91.9 (2)	Se–C–Se*	17.3 (3)
N'11–Fe–N21	90.5 (2)		
Fe–N11–N12	124.4 (3)	Fe–N21–N22	123.9 (3)
Fe–N11–C15	127.3 (3)	Fe–N21–C25	127.1 (4)
C15–N11–N12	108.1 (4)	C25–N21–N22	108.9 (4)
N11–N12–C13	106.2 (4)	N21–N22–C23	106.0 (4)
N12–C13–N14	109.8 (5)	N22–C23–N24	109.7 (5)
N12–C13–H13	126 (4)	N22–C23–H23	128 (4)
N14–C13–H13	126 (4)	N24–C23–H23	123 (4)
C13–N14–C15	107.4 (4)	C23–N24–C25	106.9 (4)
N14–C15–N11	108.5 (5)	N24–C25–N21	108.4 (5)
N14–C15–H15	132 (4)	N24–C25–H25	126 (4)
N11–C15–H15	119 (4)	N21–C25–H25	125 (4)
C13–N14–N24	127.7 (4)	C23–N24–N14	127.4 (4)
C15–N14–N24	127.8 (4)	C25–N24–N14	125.5 (4)

Hydrogen-Bonding System			
Distances			
O–H	0.88 (8)	H–N22	2.34 (9)
O–N22	3.167 (4)		
Angle			
H–O–H'		99 (12)	

In both cases, the more linear setup is associated with the shorter C–Se bond, 1.778 (7) Å compared to 1.85 (1) Å. For $Fe(btr)_2(SeCN)_2 \cdot H_2O$, only one oxygen position could be located although the thermal parameters for that one position are extremely high. The similarity of bond lengths, bond angles, and positions of the hydrogen-bridge system is notable. Thus for example, the H–O bond is found to be 0.88 (8) Å compared to 0.9 (1) Å for the cobalt analogue, the HOH angle is 99 (12)°, and the H–N22 distance is 2.34 (9) Å compared to 2.3 (1) Å.[1]

B. EPR Results. Both $Fe(btr)_2(SCN)_2 \cdot H_2O$ and $Fe(btr)_2$-$(SeCN)_2 \cdot H_2O$ were prepared with small amounts of the EPR active ions Cu^{2+} and Mn^{2+}. The powder spectra of both ions in $Fe(btr)_2(SeCN)_2 \cdot H_2O$ are broad above the spin-crossover temperature with indistinct characteristics, but this changes dramatically after the transition to spectra with sharp and distinct features.

The EPR spectra were fitted to the spin Hamiltonian

$$\hat{H} = \beta H \cdot g \cdot \hat{S} + D[\hat{S}_z^2 - \tfrac{1}{3}S(S+1)] + E(\hat{S}_x^2 - \hat{S}_y^2) +$$
$$(a/6)\{\hat{S}_x^4 + \hat{S}_y^4 + \hat{S}_z^4 - \tfrac{1}{5}S(S+1)[3S(S+1) - 1]\} + \hat{S} \cdot A \cdot \hat{I}$$
$$(1)$$

where the zero-field parameters D, E, and a apply only to ions with $S > \frac{1}{2}$ such as Mn^{2+}, for which $S = \frac{5}{2}$. These parameters are zero for Cu^{2+} for which $S = \frac{1}{2}$.

Complexes Doped with Copper. Very broad and completely unresolved spectra could be observed for both powder and single-crystal samples above the transition temperature. We have not observed the weak signals at $g = 4.7$ and $g = 3.4$ that were reported by Vreugdenhil, et al.[8] for $Fe(btr)_2(SCN)_2 \cdot H_2O$. Extremely well-resolved spectra were observed below the transition temperature with the following values (identical parameters for both compounds) measured at 77 K; $g_\parallel = 2.280$, $g_\perp = 2.057$, $A_\parallel = 177 \times 10^{-4}$ cm^{-1}, $A_\perp \approx 0$. Hyperfine coupling of four nitrogen

atoms was clearly visible in the single crystals of Fe(btr)$_2$-(SCN)$_2$·H$_2$O as well as the copper isotope effect. Determination of the coupling constants for nitrogen is somewhat risky since the spectra near the parallel orientation are obscured by the presence of resonance lines from both copper isotopes and those near the perpendicular orientation are obscured by the small hyperfine coupling constant of copper. Also it is to be expected that the four bitriazole nitrogens around the copper atom are not all equivalent but instead form two pairs of equivalent atoms.

The EPR parameters for copper at 77 K when the host crystal is in the diamagnetic state strongly indicate that the diamagnetic phase is a different crystalline structure from that of the paramagnetic phase for two reasons. One, the EPR parameters are consistent with a copper ion in an elongated octahedral coordination sphere with the elongation on the z axis whereas the X-ray structure of the paramagnetic form of both Fe(btr)$_2$(SCN)$_2$·H$_2$O and Fe(btr)$_2$(SeCN)$_2$·H$_2$O shows a compressed octahedron with the two Cu–NCS(Se) bonds shorter than four Cu–N ligand bonds. This elongation may be caused by a change in the crystal structure or by the Jahn–Teller effect. Two, in the single-crystal spectra (77 K) of Cu^{2+} in Fe(btr)$_2$(SCN)$_2$·H$_2$O only one spectrum is observed at all orientations while according to the X-ray structure of the paramagnetic form two spectra due to two differently oriented molecular entities are expected at most orientations. (The unit cell contains two FeN$_4$ sites whose normals to the plane make an angle of 12° to each other.) The calculated difference in position of these two spectra should be as large as 50 G at some orientations if we assume that $g_\parallel$ for copper is along these normals. These facts are best accounted for by assuming that a crystallographic phase transition occurs during the spin-crossover transition, and in the new space group, all MN$_4$ planes are parallel. Unfortunately, we are unable to check if there are two copper resonances above the transition temperature because of the extremely poor quality of the spectra recorded in the paramagnetic phase. Another strong indication that a phase change indeed occurs during the crossover is the explosive pulverizing of crystals into a very fine powder when they are warmed through the crossover.

In the preceding discussion, we assumed that the copper ions replace the iron ions and that the environment of the copper ions is very similar to that of the iron ions. The structure consists of infinite layers of ligand molecules interconnected by the metal ions and should be resistant to distortion when a few copper ions replace the iron ions. The iron site appears to be the only reasonable site for a copper ion. Further, it is very unlikely that any distortion produced by insertion of a copper ion would conveniently result in all sites becoming accidentally magnetically equivalent. Finally, it should be noted that in the next section we report that all manganese ions are similarly found to be magnetically equivalent in the diamagnetic state. Manganese ions are known to prefer the octahedral sites in which iron ions are generally found.

Complexes Doped with Manganese. Powder spectra observed above the transition temperature were very broad and featureless for both the thiocyanato and selenocyanato compounds, and zero-field splitting parameters could not be calculated from the spectra. Below the transition temperature the spectra of the selenocyanato compound shows some relatively sharp features with manganese hyperfine splittings in the low magnetic field region ($g = 4$ and more). A very characteristic feature of these spectra is the lack of the central resonance at $g = 2$ ($-^1/_2 \rightarrow ^1/_2$) and of the high-field resonances. From the 77 K spectrum of the selenocyanato compound, we estimate a D value of about 0.12 cm^{-1}. The powder spectrum of the thiocyanato complex lacked enough features to allow for even an estimate of the D value.

Only the thiocyanato compound could be obtained in crystals large enough for single-crystal EPR experiments. At room temperature, the spectra were too broad at all orientations, and no ZFS parameters could be determined. The resolution improved somewhat at lower temperatures but was only good for the orientation giving the maximal fine structure splitting, which we have taken to be the Z axis. Typical spectra are shown in Figure 3. This means that we were only able to measure the D and a parameters in the spin Hamiltonian. At 170 K (above the
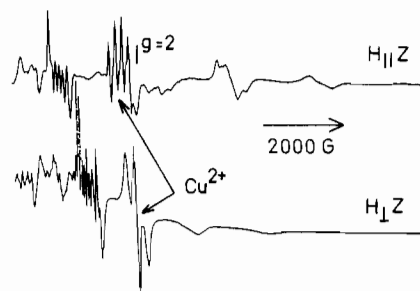

Figure 3. Single-crystal EPR spectra below the spin-crossover transition for Mn^{2+} in Fe(btr)$_2$(SCN)$_2$·H$_2$O. The resonances labeled Cu^{2+} result from an impurity in the reagents that we could not eliminate.

transition temperature), we found that $D = 0.066$ cm$^-$ and $a = 0$. When a crystal was cooled down to 110 K, slightly below the "crossover", the parameters changed to $D = 0.11$ cm^{-1} and $a = -0.0018$ cm^{-1}. Further cooling down to 77 K resulted in only a slight increase in D: $D = 0.12$ cm^{-1}, and $a = -0.0018$ cm^{-1}. Thus, the D value for the thiocyanate at 77 K is the same as that found from the powder spectrum of the selenocyanate. The spectra for the diamagnetic phase do indicate the presence of only one magnetic site as was found for the copper-doped compounds. The low quality of the spectra in the paramagnetic phase prevents any conclusions as to the number of magnetic sites in the lattice.

C. NMR Results. Temperature Dependence of Powder Spectra. In Figure 4 is shown the proton NMR spectra of powder samples of Fe(btr)$_2$(SeCN)$_2$·H$_2$O for temperatures from room temperature to temperatures well below the transition temperature. A similar figure is included in the supplementary material for Fe(btr)$_2$-(SCN)$_2$·H$_2$O as Figure S1. The spectrum in the paramagnetic phase is broad and highly anisotropic in shape, in contrast to the relatively narrow and symmetrical line shape observed in the diamagnetic phase. Although it is easy to see roughly the temperature region of the transition and the existence of hysteresis in these figures, the determination of the exact transition temperatures required a simulation analysis of the line shapes, which is considered in the Discussion below. The spectra observed in the transition region appear to be a simple summation of the paramagnetic and diamagnetic spectra, and this will be shown to be the case when the simulations are discussed.

The spectrum observed is from three types of protons. The protons of the btr ligand are of two types in that half of them are bonded to the carbon atom adjacent to the coordinating nitrogen (hereafter referred to as protons I) and the other half are bonded to the carbon atom adjacent to the noncoordinating nitrogen (hereafter referred to as protons II). The third type of proton (hereafter referred to as proton III) is found in the water of hydration molecule and is half the abundance of the other two types of protons. To help in our simulation analysis, we tried removing the water proton by precipitating the Fe(btr)$_2$(SCN)$_2$ from D$_2$O solution but found that there was considerable exchange with the ligand protons in the period of time that the compound was dissolved. We, therefore, prepared a dehydrated form of Fe(btr)$_2$(SCN)$_2$ and measured its spectrum at different temperatures down to 170 K. The dehydrated compound does not undergo a spin-crossover transition and remains paramagnetic at all temperatures measured. Finally, we also measured the room-temperature spectrum of the related Co(btr)$_2$(SCN)$_2$·H$_2$O compound.

T_1 **Measurements.** In our simulation of the powder spectrum of the paramagnetic phase, portions of the spectrum can be attributed to specific protons in certain orientations. This suggested to us that it might be of interest to study the T_1 behavior of the spectrum in different regions of the spectrum. Using the modified inversion–recovery pulse scheme of Frye,[15] we measured time-dependence decay in magnetization for specific points in the spectrum for the powder sample at room temperature. The time dependence was fitted to a double exponential decay model by using a SIMPLEX computer program. A single-exponential decay was sufficient to fit the data from the outer portions of the
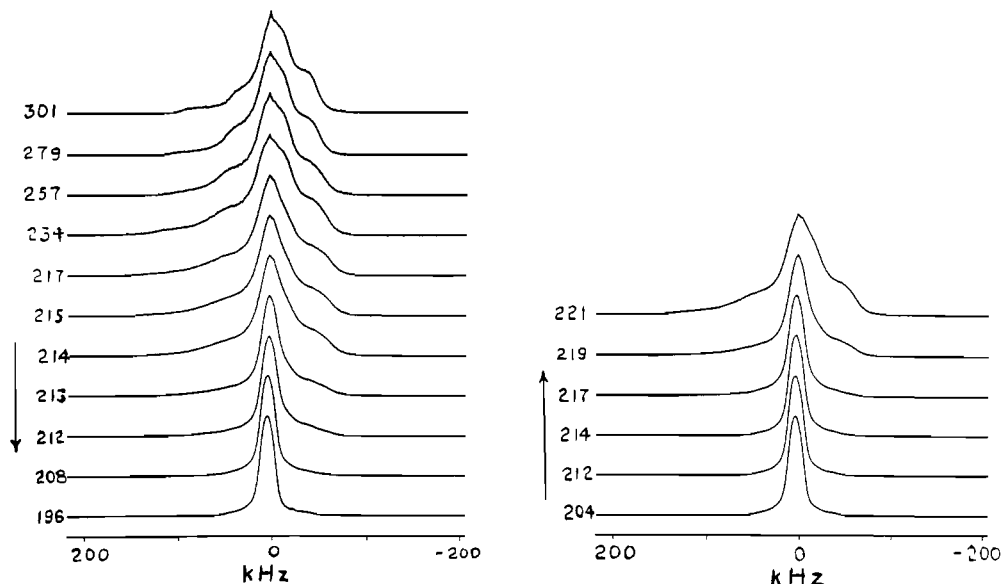
Figure 4. NMR ^{1}H spectra of Fe(btr)$_2$(SeCN)$_2$·H$_2$O (powder) at different temperatures (Kelvin). Arrows indicate the direction of change in the temperature.
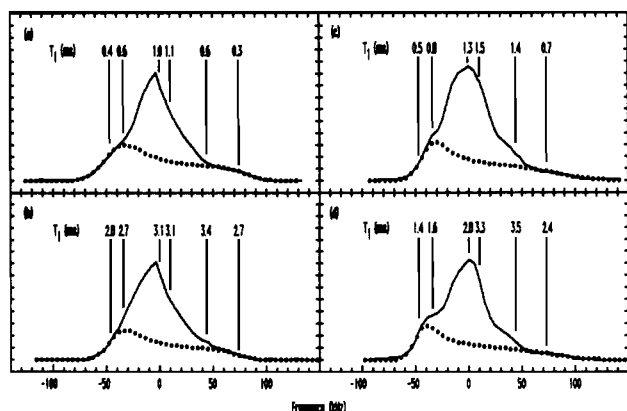

Figure 5. T_1 (in milliseconds) of ^{1}H as a function of observation frequency. Solid curve is the experimental spectrum and the circles represent the simulated spectrum for protons I in the sample. All measurements were at room temperature for all four compounds.

spectrum that could be attributed to mainly the protons of type I. A better fit was obtained with a double-exponential function for the central portions of the spectrum that is due to more than one type of proton. In all cases, the longer time component amounted to less than 10% of the total intensity. The results for the main and shorter T_1 values are displayed in Figure 5.

Simulation of NMR Powder Spectra

The anisotropic shape of the powder spectrum in the paramagnetic phase is the result of the dipolar interaction between the magnetic iron atom and the proton spin. The frequency shift $\Delta\nu$ in a solid containing many paramagnetic ions is a complicated function of the orientation of the magnetic field, which can be expressed in terms of the shift tensor $(\Delta\nu/\nu)_{ij}$. The general equation for the paramagnetic shift tensor of a nucleus interacting with several paramagnetic metal ions is[16]

$$(\Delta\nu/\nu)_{ij} = \sum_k R_k^{-3}\{3(\cos\theta_i^k)(\sum_m \chi^k_{mj}\cos\theta_m^k) - \chi^k_{ij}\} \quad (2)$$

where χ_{ij}^k is the susceptibility tensor component for the kth paramagnetic ion, $\cos\theta_i^k$ is the direction cosine of the ith vector coordinate of ion k, and R_k is the distance from the proton of the kth paramagnetic ion. This equation was derived by assuming that the lifetime of a given spin state in the metal ion is very short compared to the inverse Larmor frequency of the nucleus, which

is the case in the systems studied here. In our simulations we have assumed an isotropic susceptibility tensor, and this reduces eq 2 to

$$(\Delta\nu/\nu)_{ij} = \chi\sum_k R_k^{-3}\{3(\cos\theta_i^k)(\cos\theta_j^k) - \delta_{ij}\} \quad (3)$$

If we can assume one paramagnetic ion is much closer to the proton than all the others, the shift can be given by

$$(\Delta\nu/\nu) = \chi R^{-3}\{3\cos^2\theta - 1\} \quad (4)$$

where θ is now the angle of the magnetic field with the R vector between the proton and the paramagnetic ion.

In our simulation of the powder spectrum, we have assumed that protons I and III can be assumed to follow eq 4 but protons II follow a more complex behavior due to the closeness of the two metal ions that are bridged by the btr ligand. Thus for protons I and III, the nature of the angular variation in shift can be expressed in terms of two parameters, $(\Delta\nu/\nu)_\parallel$ and $(\Delta\nu/\nu)_\perp$, but for protons II, we will require three principal shift parameters.

In a true powder spectrum, all possible orientations of the magnetic field are equally probable statistically, giving rise to a very anisotropic spectrum. We have written a simulation program that will calculate the powder spectrum for any assumed set of three principal shifts. The program can assume the resonance of a given crystallite to be either Gaussian or Lorentzian in line shape and allows for the variation of line width with orientation in a simple manner from principal shift to principal shift. In practice, we find that only good fits are obtained with a Gaussian shape for the resonance line. The program can add different powder spectra with specified areas to simulate the sort of powder spectra found in this study. The calculated and experimental curves are compared under conditions of equal area to determine the quality of fit.

Fe(btr)$_2$(SCN)$_2$ (Dehydrated). The simulation program was tested with this system first since there are only two proton resonances (I and II) of equal intensity and it can be assumed that the parameters for I and II needed to fit the experimental spectra here will be similar to those needed for the hydrated system. The method of fitting was to first fit the outer parts of the experimental spectrum that are due to proton I to just the simulated spectrum for proton I and then subtract the simulated spectrum from the experimental spectrum. This difference spectrum was then used to determine parameters needed to simulate the spectrum for proton II. The result of this is displayed in Figure 6a for the room-temperature spectrum. The same was done for all temperatures measured. In order to obtain a good fit, it was found necessary to assume a line width variation with orientation. The
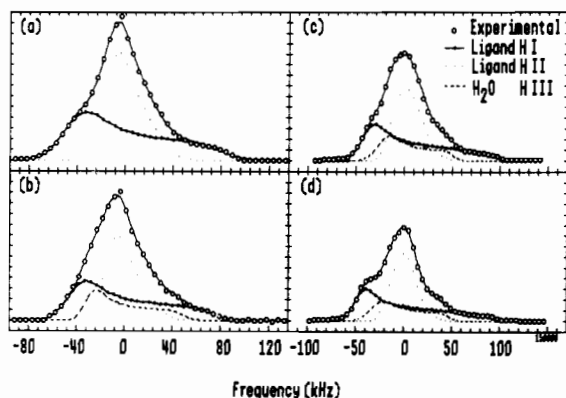
(16) Reuveni, A.; McGarvey, B. R. *J. Magn. Reson.* **1978**, *29*, 21.

Figure 6. Simulated ^{1}H NMR spectra for room-temperature powder samples of (a) Fe(btr)$_2$(SCN)$_2$ (dehydrated), (b) Co(btr)$_2$(SCN)$_2$·H$_2$O, (c) Fe(btr)$_2$(SCN)$_2$·H$_2$O, and (d) Fe(btr)$_2$(SeCN)$_2$·H$_2$O.
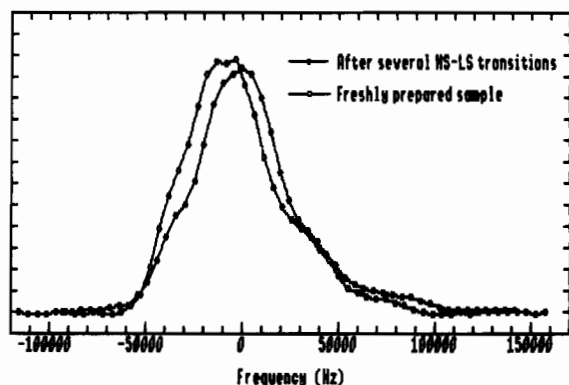
Figure 7. Comparison of ^{1}H NMR spectrum for a freshly prepared powder sample of Fe(btr)$_2$(SCN)$_2$·H$_2$O versus that of the same sample when it has been taken through the spin-crossover transition several times. Intensities of the two spectra have been adjusted to give them both the same area.

line widths were found to increase as the temperature was lowered, increasing the errors in the fitting parameters determined. The shift tensor parameters determined are given in Table SIV in the supplementary material. A plot of these parameters versus temperature reveals a discontinuity between 139 and 170 K, which could indicate a phase change.

Co(btr)$_2$(SCN)$_2$·H$_2$O. In fitting the room-temperature spectrum of this compound, we assumed the same parameters for protons I and II except that they were scaled by the ratio of the experimental atomic magnetic susceptibility of the cobalt compound[1] to that of the same iron compound.[2,3] The line widths were adjusted slightly to fit the outer parts of the spectrum. The simulated spectrum for I and II was then subtracted from the experimental spectrum and the resulting curve for III was then fitted to a simulated curve. The resulting fit is shown in Figure 6b.

Fe(btr)$_2$(SCN)$_2$·H$_2$O and Fe(btr)$_2$(SeCN)$_2$·H$_2$O. The success in fitting the above two systems gave us confidence to proceed with fitting the selenocyanato and thiocyanato spin-crossover systems studied here. The fitted room temperature spectra are shown in Figure 6c,d. Shift parameters at various temperatures are given in Table SV of the supplementary material for the paramagnetic regions of temperature. One interesting observation is that the powder spectrum for a paramagnetiic sample that has been taken through the spin-crossover transition is altered from that obtained from the sample shortly after its preparation. The room-temperature spectra of Fe(btr)$_2$(SCN)$_2$·H$_2$O before and after is shown in Figure 7. This difference could be due to the crystals in the original powder sample being too large to give a true random powder spectrum. We know from our single crystal studies that the crystals pulverize to much smaller crystallites when warmed up through the transition. Another possible explanation would be that the paramagnetic phase created by warming the dia-
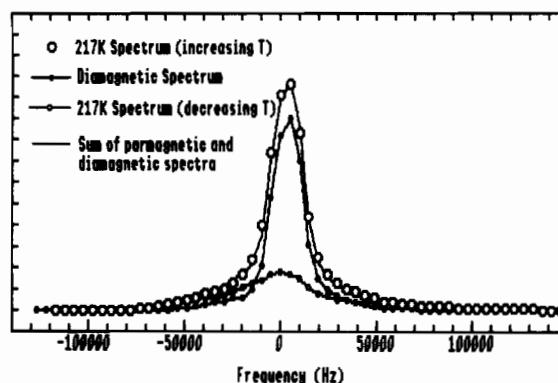

Figure 8. Demonstration that in the center of the spin-crossover transition (217 K as the temperature is raised from the diamagnetic region) the ^{1}H NMR spectrum of Fe(btr)$_2$(SeCN)$_2$·H$_2$O can be represented as a sum of the diamagnetic spectrum (measured at 196K) and the spectrum of the paramagnetic phase measured at 217K as the temperature was lowered. In the summation, the area of the diamagnetic spectrum was 65% that of the experimental curve.

magnetic phase is not the same as that obtained by crystallization from a solvent. Our fitted simulations are for samples that have been taken through the spin-crossover transition one or more times.

We have investigated the spectra in the spin-crossover region with some care because the spectra appear to be a simple sum of the diamagnetic and paramagnetic signals. To check this we have examined the 217 K spectra for Fe(btr)$_2$(SeCN)$_2$·H$_2$O taken from increasing and decreasing temperature runs. The decreasing spectrum is that of a nearly 100% paramagnetic system while the increasing spectrum is in the middle of the crossover transition. In Figure 8 is shown the result of combining the paramagnetic spectrum at 217 K with the diamagnetic spectrum obtained at 196 K, assuming the sample to be 65% diamagnetic. The excellent fit demonstrates that the intermediate spectra are indeed simple sums of the diamagnetic and paramagnetic NMR signals. In the Discussion, this observation will be used to demonstrate that the transition is not random in nature but must occur in domains or whole crystallites cooperatively.

In the region of the crossover transition, an attempt to determine the percentage of diamagnetic iron in the sample was done by using the simulation program. The experimental diamagnetic spectrum was scaled to different intensities and subtracted from the experimental spectrum in the transition region until a reasonable paramagnetic powder spectrum was obtained. The ratio of the area of the diamagnetic spectrum to the total spectrum is then taken to give the fraction of diamagnetic iron ions in the sample. It was found that this visual technique was accurate to about ±5%. A plot of the results is given in Figure 9. From these plots, we can see that the transition temperature for Fe(btr)$_2$(SCN)$_2$·H$_2$O is 125 K for decreasing temperatures and 140 K for increasing temperatures. The corresponding transition temperatures for Fe(btr)$_2$(SeCN)$_2$·H$_2$O are 211 and 217 K, respectively. These are in good agreement with the values reported from magnetic susceptibility studies. The bulk of the transition appears to occur continuously over a range of 6–8 deg rather than abruptly at one temperature.

Attempts to simulate the diamagnetic spectra of Fe(btr)$_2$-(SCN)$_2$·H$_2$O and Fe(btr)$_2$(SeCN)$_2$·H$_2$O with a simple Gaussian or Lorentzian curve were unsuccessful. The main central portion fitted a Gaussian curve very well, but the broad tails could not be fitted. An excellent fit was obtained by assuming that protons I and II gave a Gaussian curve and that protons III (H$_2$O) gave rise to a broad Pake doublet powder spectrum that had an intensity of 20% of the total resonance. The H–H distances for H$_2$O obtained from fitting the Pake portion of the spectrum are given in Table IV.

Discussion

The room-temperature X-ray structure of crystals of Fe-(btr)$_2$(SCN)$_2$·H$_2$O and Fe(btr)$_2$(SeCN)$_2$·H$_2$O grown from solution indicate that there should be two magnetically inequivalent sites
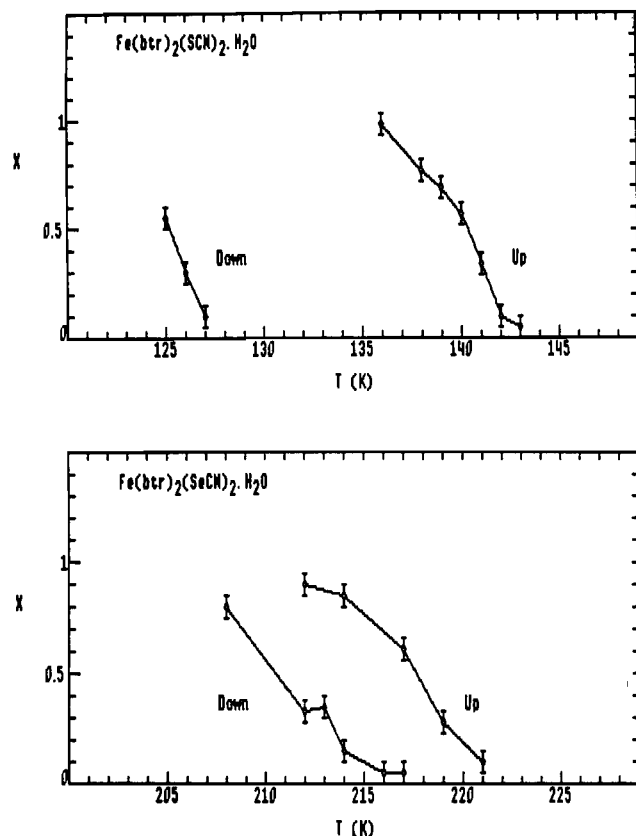
Figure 9. Variation of the mole fraction of diamagnetic phase versus temperature as measured from the NMR spectrum in the manner described in the text.

Table IV. Internuclear Distances Determined from NMR

H_2O in Diamagnetic State

	$R(H-H)$, Å	HOH angle, deg
$Fe(btr)_2(SCN)_2 \cdot H_2O$	1.46 ± 0.05	108
$Fe(btr)_2(SeCN)_2 \cdot H_2O$	1.44 ± 0.05	106

Metal–H from Paramagnetic State

	$R(M-H)$, Å	$R(M-HOH)$, Å
$Fe(btr)_2(SCN)_2 \cdot H_2O$	3.4 ± 0.1	4.0 ± 0.1
$Fe(btr)_2(SCN)_2$ (dehydrated)	3.6 ± 0.1	
$Fe(btr)_2(SeCN)_2 \cdot H_2O$	3.6 ± 0.1	4.2 ± 0.1
$Co(btr)_2(SCN)_2 \cdot H_2O$	3.4 ± 0.1	3.9 ± 0.1
$Fe(btr)_2(SeCN)_2 \cdot H_2O$ (X-ray[a])	3.3	4.3

[a] This work.

in the crystal lattice while the EPR spectra of both Cu^{2+} and Mn^{2+} in the diamagnetic phase show only one magnetic site. This fact and the explosive fracturing of the crystals when warmed from the diamagnetic to paramagnetic state are strong evidence for a phase change occurring in the spin-crossover. The distinct difference in the room-temperature powder NMR spectrum of a freshly prepared sample from the sample that has been cooled through the spin crossover and then warmed back to room temperature could be explained by there being two paramagnetic phases, one prepared by crystallization from solution and the other by warming from the diamagnetic phase. The existence of more than one phase is not unknown[7,9] in spin-crossover systems.

The demonstration that NMR spectra observed in the transition region are simple sums of the spectra observed in pure diamagnetic and paramagnetic samples is very strong evidence that the transition takes place simultaneously in domains of the crystal rather than having individual iron ions change spin state in a statistically random manner. In the paramagnetic region of temperatures, our simulations were successful using a model in which for protons I and III only the position of one iron ion was needed but for protons II the positions of two iron ions were needed. The portion

of the spectrum due to ligand protons II (40% of the total signal) in the paramagnetic state is thus determined by the magnetic moments of both of the iron ions bridged by the ligand, which are 5.1 and 6.3 Å from the proton. Consider now the sample with 50% of the iron ions diamagnetic; in a purely statistical distribution, we would have only 25% of protons II bridging two paramagnetic irons, 25% bridging two diamagnetic irons, and 50% bridging one diamagnetic iron and one paramagnetic iron. Therefore, in the statistical case, the intermediate spectrum should be the sum of three types of spectra. The fact that the intermediate spectrum was only the sum of the purely diamagnetic and purely paramagnetic spectra is then very good evidence of a domain-type transition in these systems. EPR results[7,9,10] and hysteresis studies[5a] on other systems have also given evidence of domains in spin-crossover transitions.

Since the shapes of the NMR spectra depend on the position of the different protons in the lattice, it is of interest to compare the positional data obtained from NMR with that from the X-ray studies. From the diamagnetic spectra of $Fe(btr)_2(SCN)_2 \cdot H_2O$ and $Fe(btr)_2(SeCN)_2 \cdot H_2O$, we obtained the H–H distance for the H_2O molecule given in Table IV. These are reasonable and combined with the 0.9-Å O–H distance from the X-ray work give the HOH bond angles listed in Table IV. In our simulation of the paramagnetic spectra, protons I and III were simulated by using eq 4 and the fitting parameters give us a value of (χ/R^3). Using experimental values of χ, we calculate the values of R, the distance between the proton and the iron ion, given in Table IV. The value of R given for the dehydrated sample of $Fe(btr)_2(SCN)_2$ was obtained by using the experimental value of χ obtained for the hydrated compound. The values of R agree well with what is expected from the X-ray work.

It should be noted that in our simulations of the paramagnetic spectra of $Fe(btr)_2(SCN)_2 \cdot H_2O$, $Fe(btr)_2(SeCN)_2 \cdot H_2O$, and $Co(btr)_2(SCN)_2 \cdot H_2O$, it was not necessary to include the dipole–dipole interaction between the two water protons that was needed to simulate the diamagnetic spectra. In fact, any attempt to include it made it difficult to get a reasonable fit with the experimental spectra. This could result from motional narrowing in the paramagnetic phase due to the jumping of the water protons between several orientations in the lattice. The crystal structures reported for this phase are consistent with this conclusion. The fact that the hydrogen bonding in the diamagnetic phase is large enough to prevent this motional narrowing is additional evidence that there is a structural difference between the diamagnetic and paramagnetic phases.

The T_1 results for the paramagnetic powders are very interesting and, to our knowledge, are the first data of this type to appear in the literature. For the iron(II) compounds studied, there is clear evidence that the protons closer to the magnetic iron atoms have a shorter T_1 than those further away, and the same does not appear to be true for the cobalt(II) compound. Also, the thiocyanate compound of iron(II) has much shorter T_1 values than the corresponding selenocyanate compound. These preliminary results plus the lack of temperature dependence in earlier studies on other systems suggest a mechanism other than a simple dipolar interaction. Although there has been considerable theoretical and experimental studies done of T_1 in diamagnetic solids containing paramagnetic impurities[17-22] there are no theories of T_1 in paramagnetic solids to help us interpret our results. This would appear to be an area that needs more study, and we plan to continue our T_1 work on this and related systems.

(17) Bloembergen, N. *Physica (The Hague)* **1949**, *15*, 368.
(18) Khutsishvili, G. R. *Tr. Inst. Fiziol. Akad. Nauk Gruz. SSR* **1956**, *4*, 3.
(19) De Gennes, P.-G. *J. Phys. Chem. Solids* **1958**, *7*, 345.
(20) Blumberg, W. E. *Phys. Rev.* **1960**, *119*, 79.
(21) Rorschach, H. E., Jr. *Physica (The Hague)* **1964**, *30*, 38.
(22) Lowe, I. J.; Tse, D. *Phys. Rev.* **1968**, *166*, 279.

Contribution from the Laboratoire de Chimie Inorganique (CNRS, URA 420) and Laboratoire d'Utilisation du Rayonnement Electromagnétique (CNRS, MEN, CEA), Université Paris-Sud, 91405 Orsay, France, and Laboratoire de Chimie des Métaux de Transition (CNRS, URA 419) and Laboratoire de Physique des Milieux Très Condensés (CNRS, URA 782), Université P. et M. Curie, 4 Place Jussieu, 75252 Paris Cedex 05, France

Pressure-Induced Spin-State Crossovers in Six-Coordinate Cobalt(II) Complexes: A Near-Edge X-ray Absorption Study

C. Roux,[1a] J. Zarembowitch,*,[1a] J. P. Itié,*,[1b] M. Verdaguer,[1c,d] E. Dartyge,[1d] A. Fontaine,[1d] and H. Tolentino[1d]

The pressure-induced cobalt(II) high-spin (HS) ↔ low-spin (LS) crossover has been investigated at room temperature in six-coordinate complexes of the type Co(H$_2$fsa$_2$en)L$_2$, where H$_2$fsa$_2$en^{2-} is the phenolic dianion of the Schiff base resulting from the 2:1 condensation of 3-carboxysalicylaldehyde with 1,2-diaminoethane and L is an axial ligand. The transition was followed at room temperature by near-edge X-ray absorption (XANES) spectroscopy. It was found to require the application of pressures lower than 1.1 GPa for compounds **1** (L = pyridine), **2** (L = 4-*tert*-butylpyridine), and **3** (L = H$_2$O), which are known to present a thermally driven spin conversion, and to occur between ~6.5 and ~9.0 GPa for compound **4** (L = 3-methylpyridine), which retains the HS form at any temperature. Plots of the LS fraction (n_{LS}) as a function of pressure could be deduced from the data. The phenomenon was found to be reversible (but for **3**, which probably undergoes a slight decomposition under pressure) and the HS → LS transformation to be nearly complete. Moreover, the molecular structures of the two spin forms were shown to be practically independent of pressure and hence of the LS fraction. The differences in transition pressure are discussed in terms of ligand-field strength and of strengthening of intermolecular hydrogen bonds when pressure is applied. The spectral changes associated with the spin conversion are interpreted.

Introduction

In a number of transition-metal molecular compounds, the ligand-field strength happens to have the same order of magnitude as the mean electron-pairing energy. The metal ion is then capable of undergoing a spin-state interconversion under the effect of an external perturbation.[2-8] The transition from the high-spin (HS) to the low-spin (LS) form is known to be accompanied by a shortening of the metal–ligand distances, which generally leads to a decrease in the molecular volume and hence in the crystal unit-cell volume, the reverse holding true in the case of a LS to HS conversion.[9] Pressure may act as the external perturbation, the system being then thermodynamically governed at constant temperature by $(\partial G/\partial P)_T$, which corresponds to volume (G = Gibbs free energy, P = pressure). However pressure-induced spin crossovers in solid-state molecular compounds have not yet been

as widely investigated as thermally driven ones. Furthermore, most of the studies reported to date are relative to iron(II) complexes (as examples, see refs. 10-22). Only two of them deal with cobalt(II) compounds, viz. the five-coordinate species Co(nnp)$_2$(NCS)$_2$, where nnp = *N*-((diphenylphosphino)ethyl)-*N'*,-*N'*-diethylethylenediamine,[23] and tetrahedral complexes of the type Cs$_2$CoX$_4$ (X = Cl, Br, I).[24]

In this paper, we present the first pressure-induced $S = \frac{3}{2} \leftrightarrow S = \frac{1}{2}$ transitions in six-coordinate cobalt(II) complexes. The

(1) (a) Laboratoire de Chimie Inorganique, Université Paris-Sud. (b) Laboratoire d'Utilisation du Rayonnement Electromagnétique, Université Paris-Sud. (c) Laboratoire de Chimie des Métaux de Transition, Université P. et M. Curie. (d) Laboratoire de Physique des Milieux Très Condensés, Université P. et M. Curie.
(2) Gütlich, P. *Struct. Bonding (Berlin)* **1981**, *44*, 83–202.
(3) König, E.; Ritter, G.; Kulshreshtha, S. K. *Chem. Rev.* **1985**, *85*, 219–234.
(4) Rao, C. N. R. *Int. Rev. Phys. Chem.* **1985**, *4*, 19–38.
(5) Bacci, M. *Coord. Chem. Rev.* **1988**, *86*, 245–271.
(6) Beattie, J. K. *Adv. Inorg. Chem.* **1988**, *32*, 1–53.
(7) Toftlund, H. *Coord. Chem. Rev.* **1989**, *94*, 67–108.
(8) Gütlich, P. *Coord. Chem. Rev.* **1990**, *97*, 1–22.
(9) König, E. *Prog. Inorg. Chem.* **1987**, *35*, 527–622.
(10) Fisher, D. C.; Drickamer, H. G. *J. Chem. Phys.* **1971**, *54*, 4825.
(11) Bargeron, C. B.; Drickamer, H. G. *J. Chem. Phys.* **1971**, *55*, 3471.
(12) Ferraro, J. R.; Takemoto, J. *Appl. Spectrosc.* **1974**, *28*, 66.
(13) Butcher, R. J.; Ferraro, J. R.; Sinn, E. *Inorg. Chem.* **1976**, *15*, 2077.
(14) Haller, K. J.; Johnson, P. L.; Feltham, R. D.; Enemark, J. H.; Ferraro, J. R.; Basile, L. J. *Inorg. Chim. Acta* **1979**, *33*, 119.
(15) Long, G. J.; Becker, L. W.; Hutchinson, B. B. *Adv. Chem. Ser.* **1981**, *194*, 453.
(16) Adams, D. M.; Long, G. J.; Williams, A. D. *Inorg. Chem.* **1982**, *21*, 1049.
(17) Pebler, J. *Inorg. Chem.* **1983**, *22*, 4125.
(18) Usha, S.; Srinivasan, R.; Rao, C. N. R. *Chem. Phys.* **1985**, *100*, 447.
(19) Long, G. J.; Hutchinson, B. B. *Inorg. Chem.* **1987**, *26*, 608.
(20) McCusker, J. K.; Zvagulis, M.; Drickamer, H. G.; Hendrickson, D. N. *Inorg. Chem.* **1989**, *28*, 1380.
(21) Köhler, J.; Jakobi, R.; Meissner, E.; Wiehl, L.; Spiering, H.; Gütlich, P. *J. Phys. Chem. Solids* **1990**, *51*, 239.
(22) König, E.; Ritter, G.; Kulshreshtha, S. K.; Waigel, J.; Goodwin, H. A. *Inorg. Chem.* **1984**, *23*, 1896. König, E.; Ritter, G.; Waigel, J.; Goodwin, H. A. *J. Chem. Phys.* **1985**, *83*, 3055.
(23) Sacconi, L.; Ferraro, J. R. *Inorg. Chim. Acta* **1974**, *9*, 49.
(24) Stephens, D. R.; Drickamer, H. G. *J. Chem. Phys.* **1961**, *35*, 429.